Inorganic Chemistry

Article

pubs.acs.org/IC

Cationic Iridium Complexes with Intramolecular $\pi-\pi$ Interaction and Enhanced Steric Hindrance for Solid-State Light-Emitting Electrochemical Cells

Hsiao-Fan Chen,[†] Wen-Yi Hung,*[,‡] Shou-Wei Chen,[‡] Ting-Chih Wang,[†] Shih-Wei Lin,[†] Shu-Hua Chou,[†] Chih-Teng Liao,[§] Hai-Ching Su,*[,§] Hsiao-An Pan,[†] Pi-Tai Chou,*[,†] Yi-Hung Liu,[†] and Ken-Tsung Wong*[,†]

[†]Department of Chemistry, National Taiwan University, Taipei 10617, Taiwan

[‡]Institute of Optoelectronic Sciences, National Taiwan Ocean University, Keelung 20224, Taiwan

[§]Institute of Lighting and Energy Photonics, National Chiao Tung University, Tainan 71150, Taiwan

Supporting Information

ABSTRACT: Cationic iridium complexes incorporated 4,5-diaza-9,9′-spirobifluorene as N^N ancillary ligands, in which one (**2**) or two (**3**) phenyl groups were introduced onto 4,5-diazafluorene to afford intraligand $\pi-\pi$ interactions. The X-ray crystal structures of complexes **2** and **3** show that the pendant phenyl ring forms strong intramolecular face-to-face π-stacking with the difluorophenyl ring of the cyclometalated ligand with distances of 3.38 Å for complex **2** and 3.40 and 3.46 Å for complex **3**. This $\pi-\pi$ stacking interaction minimizes the expansion of the metal−ligand bonds in the excited state, resulting in a longer device lifetime in the light-emitting electrochemical cell (LEC) devices.

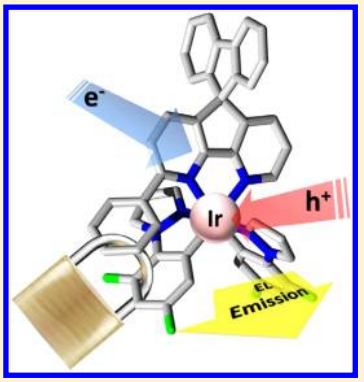

INTRODUCTION

LECs (light-emitting electrochemical cells) possess several advantages over conventional OLEDs, such as compatibility with air-stable electrodes (e.g., Ag and Au) and single emissive layer which can be easily conducted from a cost-effective solution process.[1] The turn-on voltages of LEC devices are generally low and approximately equal to the measured optical band gaps of the emissive materials (close to E_g). The low operating voltages are beneficial for the device power efficiencies. In addition to polymer-based LECs, the use of small-molecule ionic transition metal complexes (iTMCs) in LECs have attracted much attention in recent years.[2,3] In such devices, no ion-conducting material is needed because these metal complexes are intrinsically ionic. Furthermore, higher electroluminescence efficiencies are expected owing to the phosphorescent nature of the metal complexes.

Although iTMC LECs possess several promising advantages, there are still two important barriers that limit their practical application, that is, poor device stability (expressed as $t_{1/2}$, the time for the brightness of the device to decay from the maximum to half of the maximum) and long turn-on time (defined as the time required to reach a brightness of 1 cd cm^{-2}). The intrinsic instability of iTMC is attributed to a water-assisted ligand exchange reaction during the device operation, subsequently forming a new complex for efficient luminance quenching.[4] Recently, Bolink et al. demonstrated that the device lifetime can be significantly improved by increasing the hydrophobicity of the complex by introducing peripheral bulky aromatic groups. The pendant bulky group forms a face-to-face $\pi-\pi$ stacking with the metalated ring of the ligand and thus minimizes the expansion of the metal−ligand bonds in the excited state, as well as precludes the ligand exchange by foreign substances such as water. With such a molecular design, the device lifetime can significantly reach to thousands of hours.[5]

Excited state self-quenching and triplet−triplet annihilation within the solid film are well-known for devastating photoluminescent efficiency and the device lifetime due to close intermolecular packing. An efficient way to circumvent the close packing motif is to introduce steric bulky ligands. Therefore, the nonradiative pathways can be largely suppressed with increased intermolecular distance.[6] We have realized highly efficient LECs based on cationic iridium complexes with enhanced steric hindrance provided by bulky 4,5-diaza-9,9′-spirobifluorene (sp) ligand.[7] The spiro-configured structure of sp ligand has a substantial effect in preventing the intermolecular interaction, as indicated by the closest Ir-to-Ir distance larger than 8.62 Å.[8] To achieve robust cationic iridium complexes constructed by intramolecular $\pi-\pi$ interaction with enhanced steric hindrance, in this contribution we introduced

Received: March 31, 2012
Published: October 26, 2012

   dx.doi.org/10.1021/ic300673k | *Inorg. Chem.* 2012, 51, 12114−12121

Scheme 1. Synthetic Pathways and Structures of phsp, diphsp, and Complexes 1−3

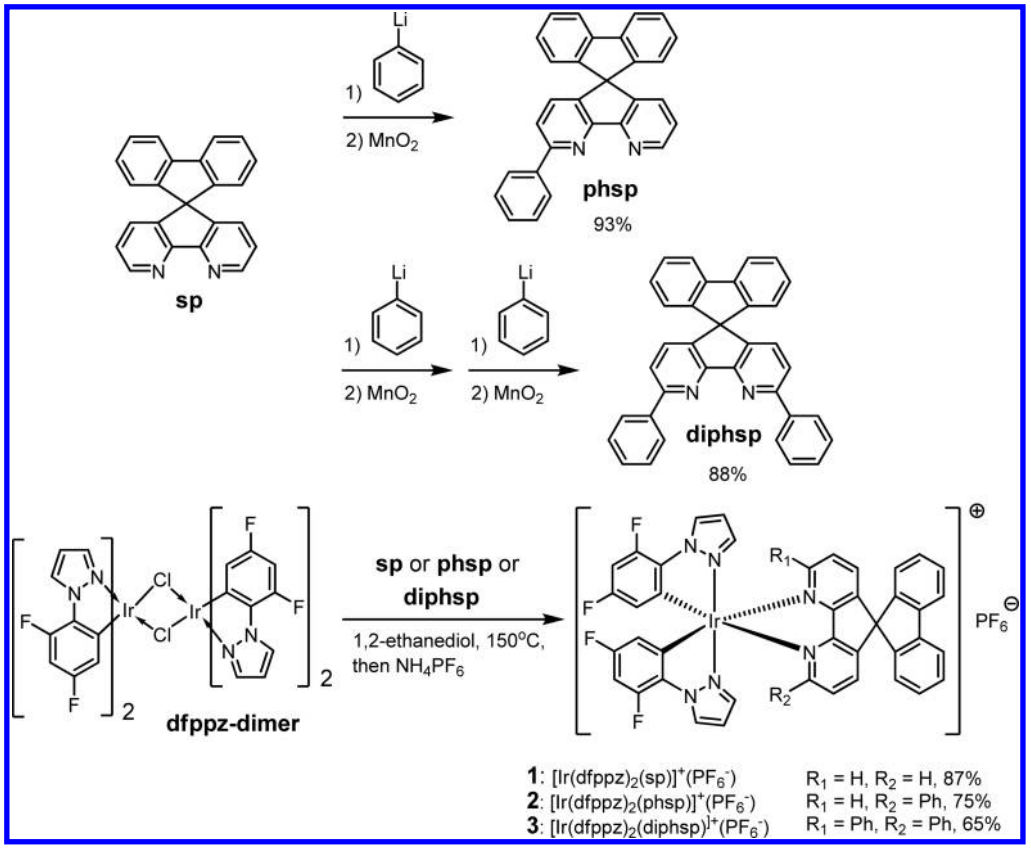

one or two pendant phenyl group at 3 and 6 positions of sp to give 3-phenyl-4,5-diaza-9,9′-spirobifluorene (phsp) and 3,6-diphenyl-4,5-diaza-9,9′-spirobifluorene (diphsp), respectively. Furthermore, in order to obtain better intramolecular cofacial $\pi-\pi$ interaction, the electron-deficient cyclometalated C^N ligand, 1-(2,4-difluorophenyl)pyrazole (dfppz), was selected for π-acceptor. The cationic iridium complexes incorporating phsp ($[Ir(dfppz)_2(phsp)]^+(PF_6^-)$, **2**) and diphsp ($[Ir(dfppz)_2(diphsp)]^+(PF_6^-)$, **3**) ligands were synthesized according to the reported synthetic route.[8] Complex without pendant phenyl group ($[Ir(dfppz)_2(sp)]^+(PF_6^-)$, **1**) was also synthesized for comparison (Scheme 1). The distances of the face-to-face $\pi-\pi$ interactions were measured to be 3.38 Å for complex **2** and 3.40 and 3.46 Å for complex **3**. This $\pi-\pi$ stacking interaction minimizes the expansion of the metal−ligand bonds in the excited state, resulting in a longer device lifetime in the LEC devices, wherein the device based on **2** showed a 4-fold lifetime enhancement as compared to that of the device based on **1**.

EXPERIMENTAL SECTION

General Experiments. ^1H and ^{13}C NMR spectra of compounds were collected on a 400 MHz spectrometer at room temperature. UV−vis absorption spectra were recorded on a spectrophotometer (Hitachi U2800A). PL spectra were measured with a fluorescence spectrophotometer (Hitachi F4500). Photoluminescence quantum yields (PLQYs) for solution and thin-film samples were determined with a calibrated integrating sphere system (Hamamatsu C9920). Phosphorescence lifetime measurements were performed with an Edinburgh FL 900 photon-counting system. Elemental analyses for diphsp were carried out on a Heraeus Vario EL III elemental analyzer at NSC Regional Advanced Instrument Center, National Taiwan University. Mass spectra were recorded on a JEOL JMS-700 mass spectrometer. Redox potentials of all complexs were determined by cyclic voltammetry (CV) at a scan rate of 100 mV/s in acetonitrile solutions (1.0 mM). A glassy carbon electrode and a platinum wire were used as the working electrode and the counter electrode, respectively. All potentials were recorded versus the Ag/AgCl (saturated) reference electrode and calibrated with the ferrocene/ferrocenium redox couple. Oxidation CV was performed using 0.1 M tetra-*n*-butylammonium hexafluorophosphate ($TBAPF_6$) in acetonitrile as the supporting electrolyte. For reduction CV, 0.1 M of tetra-*n*-butylammonium perchlorate (TBAP) in acetonitrile was used as the supporting electrolyte. Cyclometalated Ir(III) dichlorobridged dimer, bis-(μ)-chlorotetrakis(1-(4,6-difluorophenyl)-pyrazolato-C^2,N)-diiridium(III), was synthesized by a literature procedure.[9] 4,5-Diaza-9,9′-spirobifluorene (sp)[7] and complex **1**[2c] were obtained according to our previous publication.

Synthesis of 3-Phenyl-4,5-diaza-9,9′-spirobifluorene (phsp). A mixture of 4,5-diaza-9,9′-spirobifluorene (2.5 g, 7.86 mmol) and diethyl ether (400 mL) was stirred at room temperature, and phenyllithium (9.83 mL, 19.65 mmol, 2 M) was added in one portion. The reaction was stirred for 16 h, quenched with water, and extracted with diethyl ether. The organic layer was then concentrated and dissolved in CH_2Cl_2 (300 mL). Activated MnO_2 (4.78 g, 55 mmol) was added to the solution and stirred for 3 h. The mixture was filtered off through and successively washed with CH_2Cl_2 (3 × 100 mL), $CHCl_3$ (3 × 100 mL), and EtOAc (3 × 100 mL) to afford ligand phsp (2.88 g, 93%) as a pale yellow solid. Mp 229 °C (DSC). ^1H NMR ($CDCl_3$, 400 MHz) δ 8.79 (d, J = 2.8 Hz, 1H), 8.22 (d, J = 7.6 Hz, 2H), 7.88 (d, J = 7.6 Hz, 2H), 7.60 (d, J = 7.6 Hz, 1H), 7.49 (t, J = 7.6 Hz, 2H), 7.45−7.40 (m, 3H), 7.20−7.13 (m, 5H), 6.78 (d, J = 7.6 Hz, 2H). ^{13}C NMR ($CDCl_3$, 100 MHz) δ 159.1, 158.9, 158.3, 150.2, 146.2, 144.2, 142.2, 141.9, 138.9, 132.4, 131.9, 129.1, 128.6, 128.4, 128.2, 127.4, 123.9, 123.6, 120.8, 120.4, 61.4. HRMS (m/z, ESI^+) calcd for $C_{29}H_{18}N_2$ 394.1470, found 394.1473.

Synthesis of 3,6-Diphenyl-4,5-diaza-9,9′-spirobifluorene (diphsp). A mixture of 4,5-diaza-9,9′-spirobifluorene (500 mg, 1.57

dx.doi.org/10.1021/ic300673k | Inorg. Chem. 2012, 51, 12114−12121

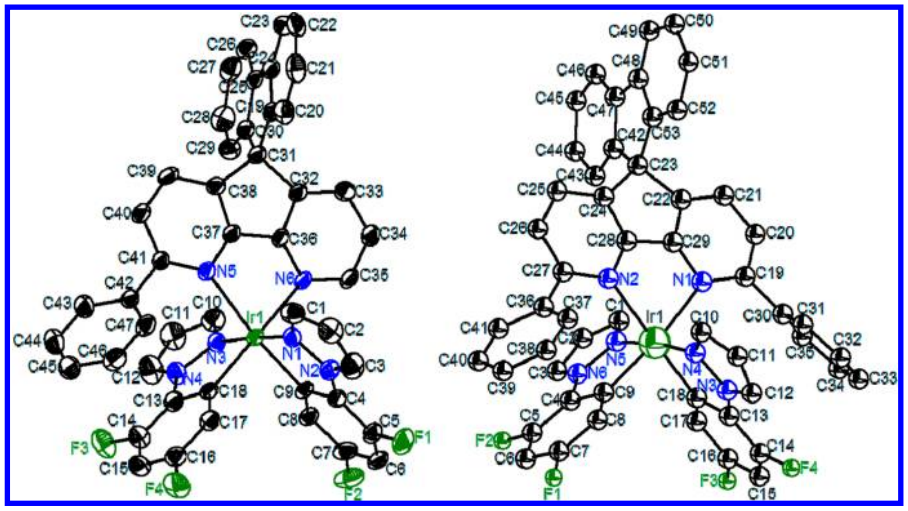

Figure 1. Crystal structures of complex **2** (left) and **3** (right). Counteranion PF_6^- and hydrogen atoms are omitted for clarity. Thermal ellipsoids are drawn at the 50% probability.

mmol) and diethyl ether (80 mL) was stirred at room temperature, and phenyllithium (2 mL, 3.93 mmol, 1.92 M) was added in one portion. After 3 h, the reaction was quenched with water and extracted with diethyl ether. The organic layer was stirred with activated MnO_2 (1.36 g) for 6 h. The mixture was dried over $MgSO_4$ and then filtered to afford 3-phenyl-4,5-diazaspirobifluorene. The target molecule was obtained by repeating the same procedure. The crude product was purified by column chromatography on silica gel (EtOAc/hexane = 1/2) to afford diphsp (650 mg, 88%) as a pale yellow solid. Mp 335 °C (DSC). ^{1}H NMR ($CDCl_3$, 400 MHz) δ 8.22 (d, J = 7.6 Hz, 4H), 7.89 (d, J = 7.6 Hz, 2H), 7.60 (d, J = 7.6 Hz, 2H), 7.50 (t, J = 7.6 Hz, 4H), 7.46−7.42 (m, 4H), 7.22−7.15 (m, 4H), 6.83 (d, J = 7.2 Hz, 2H). ^{13}C NMR ($CDCl_3$, 100 MHz) δ 159.2, 158.4, 146.4, 142.8, 141.9, 139.1, 132.4, 129.1, 128.6, 128.4, 128.2, 127.4, 123.9, 120.8, 120.4, 61.1. HRMS (m/z, ESI$^+$) calcd for $C_{35}H_{22}N_2$ 470.1783, found 470.1780; Anal. Calcd for $C_{35}H_{22}N_2$: C, 89.33; H, 4.71; N, 5.95. Found: C, 89.21; H, 4.59; N, 5.75.

Synthesis of [Ir(dfppz)$_2$(phsp)]$^+$(PF$_6^-$) (2). Bis-(μ)-chlorotetrakis(1-(4,6-difluorophenyl)-pyrazolato-C^2,N)diiridium(III) (585 mg, 0.5 mmol) and 3-phenyl-4,5-diaza-9,9′-spirobifluorene (433 mg, 1.1 mmol) were dissolved in 1,2-ethanediol (35 mL) under Ar, and the mixture was kept at 150 °C for 16 h. The solution was cooled to room temperature, and an aqueous solution of NH_4PF_6 (1.2 g in 10 mL deionic water) was added to yield yellow suspension. The solid was then filtered and dried in an oven (80 °C) for 12 h. The crude product was purified by column chromatography on silica gel (CH_2Cl_2/MeCN = 10/1) to give complex **2** (817 mg, 75%) as an yellow solid. ^{1}H NMR ($CDCl_3$, 400 MHz) δ 8.43 (d, J = 2.8 Hz, 1H), 8.31 (d, J = 2.8 Hz, 1H), 7.88 (dd, J = 8.0, 3.2 Hz, 2H), 7.69 (d, J = 5.2 Hz, 1H), 7.54−7.39 (m, 6H), 7.23−7.24 (m, 4H), 7.12 (t, J = 8.0, 1H), 7.02−6.99 (m, 3H), 6.86−6.78 (m, 5H), 6.63 (td, J = 8.0, 2.4 Hz, 1H), 6.28 (td, J = 8.0, 2.4 Hz, 1H), 5.58 (dd, J = 8.0, 2.4 Hz, 1H), 4.97 (dd, J = 8.0, 2.4 Hz, 1H). MS (m/z, ESI$^+$) 551 (50), 945 (100). HRMS (m/z, FAB$^+$) calcd for $C_{47}H_{28}F_4IrN_6$ 945.1935, found: 945.1942.

Synthesis of [Ir(dfppz)$_2$(diphsp)]$^+$(PF$_6^-$) (3). Bis-(μ)-chlorotetrakis(1-(4,6-difluorophenyl)-pyrazolato-C^2,N)diiridium(III) (585 mg, 0.5 mmol) and 3,6-diphenyl-4,5-diaza-9,9′-spirobifluorene (517 mg, 1.1 mmol) were dissolved in 1,2-ethanediol (35 mL) under Ar, and the mixture was kept at 150 °C for 16 h. The solution was cooled to room temperature, and an aqueous solution of NH_4PF_6 (1.2 g in 10 mL deionic water) was added to yield a yellow suspension. The solid was then filtered and dried in an oven (80 °C) for 12 h. The crude product was purified by column chromatography on silica gel (CH_2Cl_2/MeCN = 10/1) to give complex **3** (758 mg, 65%) as a yellow solid. ^{1}H NMR ($CDCl_3$, 400 MHz) δ 8.32 (d, J = 2.4 Hz, 2H), 7.90 (d, J = 8.0 Hz, 2H), 7.65 (d, J = 1.6 Hz, 2H), 7.50 (t, J = 7.2 Hz, 2H), 7.42 (d, J = 8.0, 2H), 7.32 (t, J = 7.2 Hz, 2H), 7.20 (d, J = 8.0, 2H), 7.19−7.08 (m, 4H), 7.02 (t, J = 8.0, 4H), 6.88 (t, J = 2.4 Hz, 2H), 6.84 (d, J = 7.2, 4H), 6.11 (td, J = 8.0, 2.4 Hz, 2H), 4.68 (dd, J = 8.0, 2.4 Hz, 2H). MS (m/z, ESI$^+$) 551 (100), 577 (95), 1021 (80). HRMS (m/z, FAB$^+$) calcd for $C_{53}H_{32}F_4IrN_6$ 1021.2248, found 1021.2236.

Crystal Structure Determinations. Crystallographic data were collected at 295(2) K on a NONIUS Kappa CCD diffractometer using graphite-monochromatized Mo Kα radiation (λ = 0.710 73 Å). Cell parameters were retrieved and refined using HKL Denzo and Scalepack software on all observed reflections.[10] Data reduction was performed with the HKL Denzo and Scalepack software. The structures were solved and refined with SHELX programs.[11] The hydrogen atoms were included in calculated positions and refined using a riding mode.

Fabrication and Characterization of LEC Devices. ITO-coated glass substrates were cleaned and treated with UV/ozone prior to use. A PEDOT:PSS layer was spin-coated onto the ITO substrate, and then, the structure was baked at 150 °C for 30 min. All solution preparing and spin-coating processes were carried out in glovebox. The emissive layer (~400 nm) was spin-coated from the CH_3CN solutions of the compound (150 mg/mL). To reduce the turn-on time of the LEC device, the ionic liquid [BMIM$^+$(PF$_6^-$)] (20 wt %) was added to enhance the ionic conductivity of thin films.[12] After spin-coating the emissive layer, the samples were baked at 70 °C for 10 h in a nitrogen glovebox (oxygen and moisture levels below 1 ppm) and then subjected to thermal evaporation of a 100-nm-thick Al top contact in a vacuum chamber (ca. 10^{-6} Torr). The electrical and emission characteristics of the LEC devices were measured using a sourcemeter (Keithley 6430) and a picoammeter (Keithley 6487) equipped with a calibration Si-photodiode. All device measurements were performed under a constant bias voltage in a nitrogen glovebox.

Computational Methodology. All the calculations were using the density functional theory (DFT) with B3LYP[13] hybrid functional. Restricted and unrestricted formalisms were adopted in the singlet and triplet geometry optimization, respectively. To investigate the photophysical properties, time-dependent DFT (TDDFT) calculations were performed on the basis of the optimized structures at the ground state. A "double-ζ" quality basis set consisting of Hay and Wadt's effective core potentials (LANL2DZ)[14] was employed for the Ir(III) metal atom, and a 6-31G* basis set[15] was employed for the rest of the atoms. The relativistic effective core potential (ECP) replaced the inner core electrons of Ir(III) metal atom, leaving only the outer core valence electrons ($5s^25p^65d^6$) to be concerned. The electronic configurations of ^{3}MC (metal-centered triplet) dd states were calculated following the literature methodology.[16] In brief, the ^{3}MLCT state geometry was obtained by performing geometry optimization along the triplet state potential energy surface (PES), using the ground state optimized structure as the initial geometry. As

dx.doi.org/10.1021/ic300673k | Inorg. Chem. 2012, 51, 12114−12121

for the ^{3}MC state, because the electron densities are mainly distributed on the central metal atom, the calculation is starting with a distorted geometry, for which the metal−ligand bondings are largely elongated, such that its associated energy is expected to be far away from the global minimum along the PES, and then the geometry optimization is performed. Accordingly, the optimization is able to fall into the presumably shallow local minimum associated with the ^{3}MC dd excited state. Moreover, considering the solvation effect, the calculations were then combined with an integral equation formalism-polarizable continuum model (in dichloromethane), IEFPCM.[17] All calculations were carried out using Gaussian 09.

RESULT AND DISCUSSION

Synthesis. Scheme 1 depicts the synthesis of the N^N ancillary ligands, phsp and diphsp. Starting from sp,[7] phsp and diphsp were synthesized in 93% and 88% yields, respectively, by nucleophilic addition (once or twice) of phenyllithium onto 4,5-diazaspirobifluorene, followed by oxidative aromatization with manganese oxide. Complexes **2** and **3** were synthesized according to the literature procedures in 75% and 65% yields, respectively.

Crystal Structures of 2 and 3. Crystals of complexes **2** and **3** suitable for the X-ray diffraction analysis were obtained by slow evaporation of the solvent from the acetone/hexane cosolvent system. The structures of complexes **2** and **3** are depicted in Figure 1, and the crystal data are summarized in Table 1. Complexes **2** and **3** both exhibit a distorted octahedral geometry around the Ir center as indicated by the small bite angles of C(9)−Ir(1)−N(1) [80.52(18)°], C(18)−Ir(1)−N(3) [79.81(17)°], and N(5)−Ir(1)−N(6) [79.87(14)°] and twisted bond angles of N(1)−Ir(1)−N(3) [175.76(14)°], C(9)−Ir(1)−N(5) [172.79(15)°], and C(18)−Ir(1)−N(6) [176.18(15)°] in complex **2**, and small bite angles of C(9)−Ir(1)−N(5) [79.87(19)°], C(18)−Ir(1)−N(4) [80.4(2)°], and N(1)−Ir(1)−N(2) [79.64(14)°] and twisted bond angles of N(4)−Ir(1)−N(5) [172.80(16)°], C(9)−Ir(1)−N(1) [170.05(17)°], and C(18)−Ir(1)−N(2) [176.70(18)°] in complex **3**. The Ir−N bond distances between the Ir center and phsp or diphsp are estimated to be Ir(1)−N(5) [2.282(4)Å], Ir(1)−N(6) [2.158(4)Å] and Ir(1)−N(1) [2.240(4)Å], Ir(1)−N(2) [2.249(4)Å], respectively, which are significantly longer than those between the Ir center and 1-(2,4-difluorophenyl)pyrazole [Ir(1)−N(1) = 2.008(4)Å, Ir(1)−N(3) = 2.010(4)Å in complex **2**, Ir(1)−N(4) = 2.028(4)Å, Ir(1)−N(5) = 2.024(4)Å in complex **3**]. This can be possibly attributed to the anionic nature of the cyclometalated 1-(2,4-difluorophenyl)pyrazole ligands, which have a stronger interaction with the cationic Ir(III) ion. The Ir−N bond distances between the Ir center and phsp or diphsp are affected by the pendant phenyl ring. The Ir−N bond is longer where the phenyl group is located. For example, the distance of Ir(1)−N(5) [2.282(4)Å] is longer than that of Ir(1)−N(6) [2.158(4)Å] in complex **2**, which is due to steric repulsion of the pendant phenyl ring. For complex **3**, two pendant phenyl rings give a comparable steric effect on both sides of Ir−N bonds, as seen with the comparable distance of Ir(1)−N(1) [2.240(4)Å] and Ir(1)−N(2) [2.249(4)Å]. The pendant phenyl rings exhibit very strong intramolecular face-to-face $\pi-\pi$ stacking with the cyclometalated difluorophenyl ring of the dfppy ligand as shown in Figure 2. The distances between two phenyl rings (the pendant phenyl ring and the cyclometalated difluorophenyl ring) are about 3.38 Å for complex **2** and 3.40 and 3.46 Å for complex **3**, indicating strong aromatic $\pi-\pi$ interaction. This interaction diminishes the possibility of foreign substances to react with the metal complex and hence reduces the possible formation of degraded products capable of quenching the luminescence. The closest Ir-to-Ir distances in complex **2** and **3** are as large as 9.47 and 9.97 Å, respectively, indicating sufficient prevention of intermolecular interaction provided by bulky 4,5-diaza-9,9′-spirobifluorene ligand.

Table 1. Crystal Data of Complexes 2 and 3

	2	3
empirical formula	$C_{48}H_{28}F_{10}IrN_6P$	$C_{53}H_{32}F_{10}IrN_6P$
fw	1174.85	1208.48
cryst dimensions (mm^3)	0.25 × 0.15 × 0.10	0.25 × 0.20 × 0.10
cryst syst	triclinic	monoclinic
space group	$P\bar{1}$	$P2_1/c$
a (Å)	12.4320(2)	16.3211(7)
b (Å)	13.5430(2)	16.8506(5)
c (Å)	13.9288(3)	19.4315(10)
α (deg)	74.532(2)	90
β (deg)	85.7760(10)	114.738(6)
γ (deg)	79.5890(10)	90
cell volume (Å)^3	2222.19(7)	4853.6(4)
Z	2	4
density (calcd) g/cm^3	1.756	1.654
F(000)	1152	2380
T (K)	295(2)	295(2)
wavelength (Å)	0.710 73	0.710 73
no. reflns collected	31 548	21 629
no. indep reflns (R_{int})	10 191(0.0415)	9698(0.0331)
$R(F)$, wR2 [$I > 2\sigma(I)$]	0.0404, 0.1089	0.0350, 0.0973
$R(F)$, wR2 (all data)	0.0536, 0.0626	0.0536, 0.1077

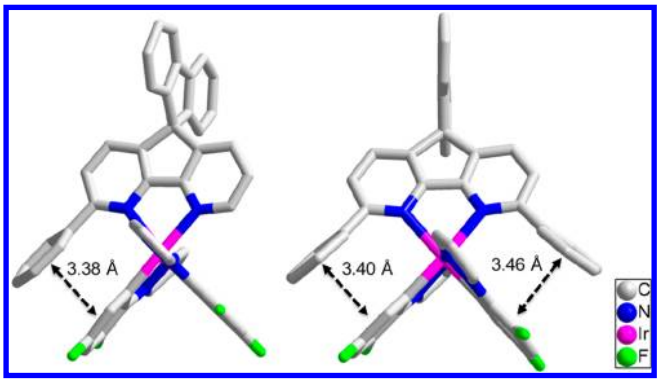

Figure 2. Face-to-face π-stacking of the pendant phenyl ring with the cylometalated difluorophenyl ring of complex **2** (left) and **3** (right). Counteranion PF_6^- and hydrogen atoms are omitted for clarity.

Photophysical Properties. Figure 3 shows the UV−vis and PL spectra of **1**, **2**, and **3** in CH_2Cl_2 (10^{-5} M) and in neat films. The photophysical properties of complexes **1**, **2**, and **3** in solutions (CH_2Cl_2, 10^{-5} M) or in thin films are summarized in Table 2. Similar absorption features were observed for all complexes. The intense absorption bands in the UV region of the spectra (240−350 nm) are associated with the ligand-centered (LC) transitions of the ligands. These LC bands are accompanied by weaker and broad bands extending from ~300 nm to the visible region, which are related to the metal-to-ligand-charge-transfer (MLCT) transitions (both allowed and spin-forbidden ones) mediated by the strong spin−orbit coupling of the Ir(III) center. In the PL spectra, all the

dx.doi.org/10.1021/ic300673k | Inorg. Chem. 2012, 51, 12114−12121

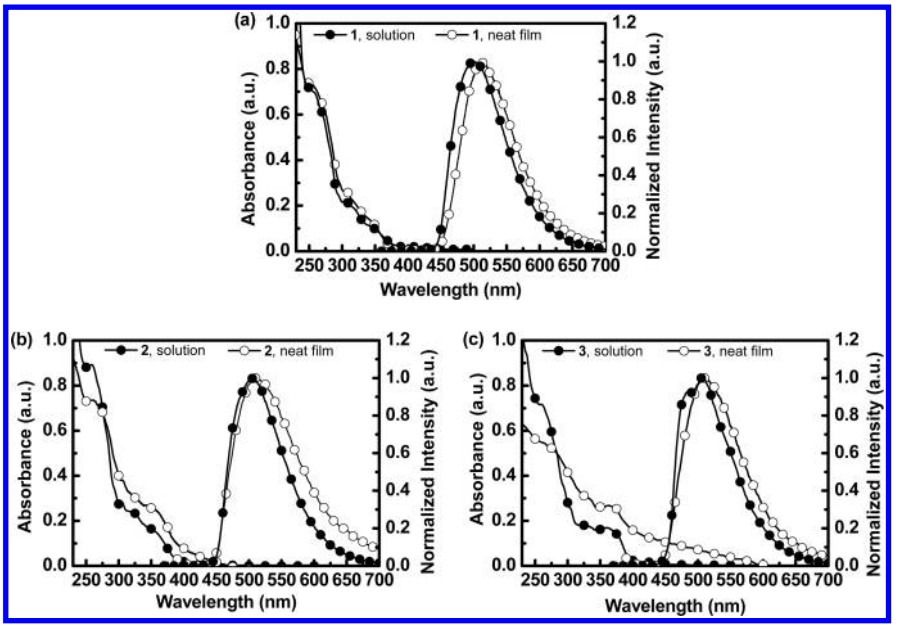

Figure 3. Absorption (left axis) and PL (right axis) spectra of (a) **1**, (b) **2**, and (c) **3** in dichloromethane solutions (10^{-5} M) and in neat films.

Table 2. Summary of Physical Properties of Complexes 1−3[a]

	λ_{PL} (nm)		PL QY					
complex	solution[b]	neat film	solution[c]	neat film	τ (μs)	k_r	k_{nr}	$E_{1/2}^{ox}/E_{1/2}^{red}$ (V)[d]
1	500	512	0.46	0.20	0.54	8.5×10^5	1.0×10^6	+1.26/−1.71
2	504	510	0.47	0.10	0.35	1.3×10^6	1.5×10^6	+1.25/−1.69
3	505	510	0.38	0.11	0.38	1.0×10^6	1.6×10^6	+1.26/−1.68

[a]At room temperature. [b]Measured in CH_2Cl_2 (10^{-5} M). [c]Measured in degassed CH_2Cl_2 solution (10^{-5} M). [d]Redox potential vs ferrocene/ferrocenium redox couple.

complexes exhibited emission maxima in the range of 500 and 505 nm. The HOMO orbital of a cationic iridium complex was reported to be a mixture of the orbitals of iridium and the phenyl group of the cyclometalated C^N ligand, whereas the LUMO orbital is generally attributed to the ancillary N^N ligand.[18] The slightly red-shifted emissions of **2** and **3** are due to larger conjugation of the N^N ligands. Intriguingly, **3** emitted with a shoulder at ~485 nm which might be attributed to the component with longer Ir−N distance between the iridium center and the ancillary N^N ligand due to the introduction of two pendant phenyl groups, causing less electron donating effect of the ancillary ligand toward the HOMO orbital. In thin films, the intermolecular interaction is dominant to the emission properties, as observed for red-shifted emission spectra of **1**, **2**, and **3** as compared with those of the PL in solutions. The slightly lower photoluminescent quantum yield (PLQY) of **3** in solution as compared to those of **1** and **2** was possibly attributed to the intraligand interactions which may facilitate the deactivation processes. By calculating the radiative and nonradiative rate constants, the introduction of one phenyl ring increases both constants by a factor of 1.5. The increase of rate constants indicates that the formation of one intramolecular $\pi-\pi$ stacking efficiently facilitates the electronic transitions between the excited states and the ground state due to enhanced molecular rigidity. However, doubling the intramolecular $\pi-\pi$ stacking significantly restricts the molecular reorganization in the excited state and thus gives less enhancement for the radiative process. In films, it is noted that both **2** and **3** exhibited much lower PLQYs than **1**, indicating that the presence of intramolecular $\pi-\pi$ stacking leads to a densely extended π-stacking in the lattice by the formation of solid-state supramolecular-caged structure.[5a]

Electrochemical Properties. Figure 4 depicts the electrochemical properties of complexes **1**−**3** probed by cyclic voltammetry (CV, see the Experimental Section for details), and the measured redox potentials versus ferrocene/ferrocenium redox couple are listed in Table 2. Notably, all complexes exhibited nearly identical redox behavior in terms of redox potentials and reversibility. A quasireversible oxidation potential for each complex was observed at around +1.25 V. The highest

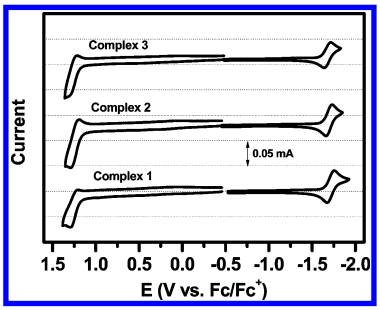

Figure 4. Cyclic voltammograms of complexes **1**−**3** in acetonitrile. 0.1 M Tetrabutylammonium hexafluorophosphate ($TBAPF_6$) and tetrabutylammonium perchlorate (TBAP) were used as supporting electrolytes for the oxidation and reduction CV, respectively. A glassy carbon electrode was used as the working electrode; scan rate 100 mV/s.

dx.doi.org/10.1021/ic300673k | Inorg. Chem. 2012, 51, 12114−12121

occupied molecular orbital (HOMO) of cationic complexes with a general formula as $[Ir(C^N)_2(N^N)]$ has been reported to be a mixture of the d orbitals of iridium and the p orbitals of the C^N ligand.[18] The similar oxidation potentials of **1**−**3** suggest that the intramolecular $\pi-\pi$ stacking does not significantly influence the electronic structure of the HOMO levels. For reduction, all complexes possess one reversible reduction peak at potentials in the range of −1.71 and −1.68 V. The reductions were unambiguously assigned to be located at the 4,5-diazafluorene moiety of the ancillary ligands of the complexes.[18] The slight difference in the reduction potentials was attributed to the different effective conjugation of the 4,5-diazafluorene upon the introduction of phenyl ring(s).

Electroluminescent Properties. Device characteristics based on the structure of the glass substrate/PEDOT:PSS/indium tin oxide (ITO)/**1** or **2** or **3** (400 nm) with 20 wt % ionic liquid/Al are discussed below and summarized in Table 3.

Table 3. Characteristics of LEC Devices Based on Complexes 1−3

3.4 V	t_{on}[a] [min]	t_{max}[b] [min]	$t_{1/2}$[c] [min]	L_{max}[d] [cd/m^2]	η_{max} [%, cd/A, lm/W]	CIE (x, y)
1	0.5	54	141	25.4	0.82, 2.13, 1.97	0.23, 0.47
2	106	390	585	5.76	1.13, 3.37, 3.12	0.28, 0.50
3	47	96	102	10.6	1.43, 4.25, 3.92	0.28, 0.54

[a]Time required to reach a brightness of 1 cd/m^2. [b]Time required to reach the maximum brightness. [c]The time for the brightness of the device to decay from the maximum to half of the maximum under a constant bias voltage. [d]Maximum brightness achieved at 3.4 voltage.

The time-dependent brightnesses of the LEC devices based on complexes **1**, **2**, and **3** operating at 3.4 V are shown in Figure 5a. The current in the device increased slowly with time after the bias was applied. The times for turning on the device (t_{on}), defined as the time to achieve a brightness of 1 cd cm^{-2}, were 0.5, 106, and 47 min for devices incorporated with complexes **1**, **2**, and **3** at 3.4 V, respectively. The brightnesses increased with current and reached the maxima of 25.4, 5.8, and 10.6 cd m^{-2} in about 54, 390, and 96 min with peak EQE value of 0.82%, 1.13%, and 1.43% for devices incorporated with complexes **1**, **2**, and **3** at 3.4 V, respectively (Figure 5b). The device lifetimes ($t_{1/2}$, defined as the time for the brightness of the device to decay from the maximum to half of the maximum under a constant bias voltage) of complexes **1**, **2**, and **3** were 141, 585, 102 min, respectively. The device based on **2** and **3** exhibited longer t_{on} and smaller current densities as compared with those of the device incorporating **1**, indicating less efficient carrier inject and/or transport (accumulation) when **2** or **3** is used as the active layer. We suggest the suppressed carrier inject and/or transport properties of **2** and **3** were attributed to the formation of solid-state supramolecular-caged structure, which results in a densely extended π-stacking in the lattice and leads to low ionic mobility.[5a] Such molecular packing motif diminished the current flux in the device and, as a result, substantially retarded the degradation of the complex and hence increased the device stability as well as EQE. Moreover, the complexes with preferable intramolecular $\pi-\pi$ interaction can "lock" the comparable labile ancillary ligand which is prone to dissociation upon electron injecting to the antibonding (π^*) orbital. As a consequence, we observed a 4-fold enhancement on the device lifetime ($t_{1/2}$) of **2** as compared to that of **1**, stemming from less current flux and enhanced molecular stability. Nevertheless, doubling the intramolecular $\pi-\pi$ interaction by two pendant groups in **3** did not render a superior device lifetime, as indicated by the shorter $t_{1/2}$ of **3** as compared to that of **1**. Costa et al. have depicted the pendant group effect of LEC performance in the 2,2′-bipyridyl system with DFT calculations.[19] The complex with two phenyl groups significantly lowers its metal-centered triplet state (^{3}MC), rendering less luminance yield for radiative decay and more probability on degradation process (*vide infra*). Therefore, although the device based on **3** possesses suppressed current flux, the unfavorable excited state process (thermal population of ^{3}MC state) still accelerated the degradation of the complex even with two intramolecular $\pi-\pi$ interactions. By inspecting the t_{on} and $t_{1/2}$ for the devices based on **1** and **2**, it is suggested that the two device properties are in a trade-off. One cannot extend a device lifetime without sacrificing the response time (i.e., t_{on}) of the device and *vice versa*. The stability of the ionic complex should be the major obstacle for obtaining high device lifetime with fast response.

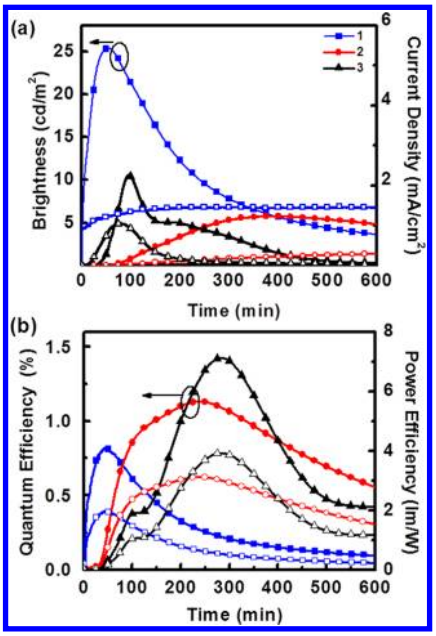

Figure 5. Dependence of (a) brightness (filled symbols) and current density (empty symbols); (b) EQE (filled symbols) and corresponding power efficiency (empty symbols).

Computational Studies. In order to understand the electronic structure of the complexes with the effect of the pendant phenyl group, we performed density functional theory (DFT) calculations at the B3LYP/(6-31G*/LANL2DZ) level on **1**, **2**, and **3** cations. The features of the frontier HOMO − 1, HOMO, and LUMO orbitals mainly involved in the lower lying electronic transitions are depicted in Figure 6. T_1 states of **1**, **2**, and **3** were calculated to lie 2.86, 2.84, and 2.80 eV above their S_0 states, respectively, which involve different contributions of electronic transitions. The dominant excitation for the T_1 states in **1**, **2**, and **3** are HOMO → LUMO (95%), HOMO → LUMO (23%) with 21% LLCT (fluorene to 4,5-diazafluorene, HOMO − 1 → LUMO), and HOMO − 1 → LUMO (34%; LLCT), respectively. We observed that the percentage of LLCT transition increases along with the number of pendant phenyl ring(s). For example, the T_1 state of **1** is mainly contributed to

dx.doi.org/10.1021/ic300673k | Inorg. Chem. 2012, 51, 12114−12121

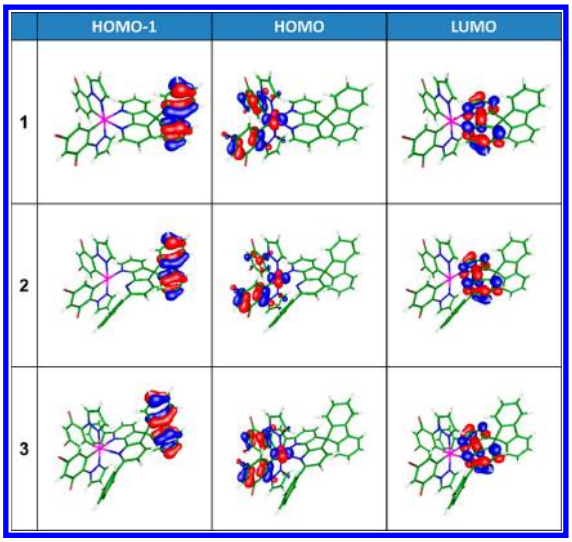

Figure 6. Frontier orbitals involved in the lower-lying electronic transitions for **1**, **2**, and **3**.

the HOMO → LUMO excitation with 26.8% MLCT (metal d_π to the 4,5-diazafluorene moiety) character, whereas the T_1 states of **2** and **3** involve higher percentage of LLCT transitions (21% and 34%, respectively). This result indicates that the dominating electronic transitions in **1**−**3** are fairly influenced by the presence of intramolecular $\pi-\pi$ stacking, restricting the molecular reorganization process in the excited state for MLCT transitions. Figure 7 illustrates the schematic energy diagram

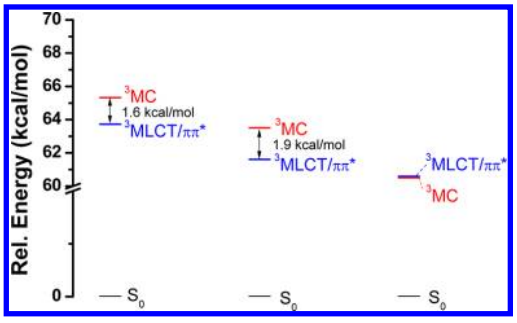

Figure 7. Schematic energy diagram showing the relative energy of the ^{3}MLCT/$\pi\pi$* and ^{3}MC excited states.

showing the relative energy of the T_1 and ^{3}MC excited states. It is noted that the T_1 and ^{3}MC excited states for **3** possess almost the same energies while the ^{3}MC excited states are higher by 1.6 and 1.9 kcal mol^{-1} for **1** and **2**, respectively. The unexpected small energy difference between T_1 and ^{3}MC excited states for **3** decreases the molecular stability through population of the ^{3}MC excited state (Table 2). Moreover, the longer Ir−N bonds between the iridium and the N^N ligand in the ^{3}MC excited states are calculated as 2.571, 2.403, and 2.707 Å for **1**, **2**, and **3**, respectively, indicating that **3** has a higher tendency to lose the ancillary ligand in the ^{3}MC excited states, in line with the shorter device lifetime of **3** as compared to that of **2**. These Ir−N bonds involve spin density on the nitrogen atoms (Figure S1). The alteration of electron distribution in the ^{3}MC excited states makes the bond lengths not simply increase with the increase of steric effect for **1** and **2**.

CONCLUSION

In summary, we have successfully synthesized two cationic iridium complexes with one or two pendant phenyl groups on the spiro-configured N^N ancillary ligand. The photophysical data revealed that the longer Ir−N distance between iridium and the ancillary ligand resulted in a blue-shifted emission spectrum due to less interaction between the ancillary ligand and the HOMO orbital (complex **3**). The X-ray crystallography shows substantial intramolecular $\pi-\pi$ interaction between pendant phenyl group and the dfppz ligand. The plane to plane distances indicating sufficient $\pi-\pi$ interaction are about 3.38 Å for complex **2** and 3.40 and 3.46 Å for complex **3**. This $\pi-\pi$ interaction minimizes the expansion of the metal−ligand bonds in the excited state and capability of preventing foreign substances to access the metal center. The LEC devices based on **2** and **3** showed much suppressed current densities which resulted from densely extended π-stacking structures. The device lifetime of the devices based on **1**, **2**, and **3** were 141, 585, 102 min, respectively. The 4-fold enhancement on the device lifetime of **2** as compared to that of **1** is benefited by less current flux and enhanced molecular stability. However, the trade-off of device response and device lifetime limits the practical use of LEC devices. The stability of the ionic complex under the electric field is considered to be the major obstacle for realizing practical LEC devices. Some possible solutions are foreseen for searching for a new type of stable molecular architecture with ionic character to allow higher durability under the electric field and developing stable neutral complexes compatible with ionic liquids to give LEC response without using degradable ionic complexes. Work related to improving LEC lifetime without sacrificing device response is under investigation and will be reported in due course.

ASSOCIATED CONTENT

Supporting Information

Additional tables, figure, and crystallographic data in CIF format. This material is available free of charge via the Internet at http://pubs.acs.org.

AUTHOR INFORMATION

Corresponding Author

*E-mail: kenwong@ntu.edu.tw (K-T.W.), wenhung@mail.ntou.edu.tw (W.-Y.H.), haichingsu@mail.nctu.edu.tw (H.-C.S.), chop@ntu.edu.tw (P.-T.C.).

Notes

The authors declare no competing financial interest.

ACKNOWLEDGMENTS

The work was supported by the financial aid of the National Science Council of Taiwan (NSC-98-2119-M-002-007-MY3 and 100-2112-M-019-002-MY3).

REFERENCES

(1) (a) Pei, Q.; Yu, G.; Zhang, C.; Yang, Y.; Heeger, A. J. *Science* **1995**, *269*, 1086. (b) Pei, Q.; Yang, Y.; Yu, G.; Zhang, C.; Heeger, A. J. *J. Am. Chem. Soc.* **1996**, *118*, 3922.

(2) (a) Lee, J. K.; Yoo, D. S.; Handy, E. S.; Rubner, M. F. *Appl. Phys. Lett.* **1996**, *69*, 1686. (b) He, L.; Duan, L.; Qiao, J.; Wang, R.; Wei, P.; Wang, L. D.; Qiu, Y. *Adv. Funct. Mater.* **2008**, *18*, 2123. (c) Colman, E. Z.; Slinker, J. D.; Parker, J. B.; Malliaras, G. G.; Bernhard, S. *Chem. Mater.* **2008**, *20*, 388. (d) Su, H.-C.; Chen, H.-F.; Fang, F.-C.; Liu, C.-C.; Wu, C.-C.; Wong, K.-T.; Liu, Y.-H.; Peng, S.-M. *J. Am. Chem. Soc.* **2008**, *130*, 3413. (e) Bolink, H. J.; Coronado, E.; Costa, R. D.; Lardiés,

N.; Ortí, E. *Inorg. Chem.* **2008**, *47*, 9149. (f) Su, H.-C.; Chen, H.-F.; Wu, C.-C.; Wong, K.-T. *Chem.—Asian J.* **2008**, *3*, 1922. (g) Kwon, T.-H.; Oh, Y. H.; Shin, I.-S.; Hong, J.-I. *Adv. Funct. Mater.* **2009**, *19*, 711. (h) He, L.; Qiao, J.; Duan, L.; Dong, G. F.; Zhang, D. Q.; Wang, L. D.; Qiu, Y. *Adv. Funct. Mater.* **2009**, *19*, 2950. (i) Costa, R. D.; Ortí, E.; Bolink, H. J.; Graber, S.; Schaffner, S.; Neuburger, M.; Housecroft, C. E.; Constable, E. C. *Adv. Funct. Mater.* **2009**, *19*, 3456. (j) Costa, R. D.; Céspedes-Guirao, F. J.; Ortí, E.; Bolink, H. J.; Gierschner, J.; Fernández-Lázaro, F.; Sastre-Santos, A. *Chem. Commun.* **2009**, 3886. (k) He, L.; Duan, L.; Qiao, J.; Dong, G.; Wang, L.; Qiu, Y. *Chem. Mater.* **2010**, *22*, 3535. (l) Costa, R. D.; Ortí, E.; Bolink, H. J.; Graber, S.; Housecroft, C. E.; Constable, E. C. *J. Am. Chem. Soc.* **2010**, *132*, 5978. (m) Costa, R. D.; Ortí, E.; Bolink, H. J.; Graber, S.; Housecroft, C. E.; Constable, E. C. *Adv. Funct. Mater.* **2010**, *20*, 1511. (n) Mydlak, M.; Bizzarri, C.; Hartmann, D.; Sarfert, W.; Schmid, G.; De Cola, L. *Adv. Funct. Mater.* **2010**, *20*, 1812. (o) Su, H.-C.; Lin, Y.-H.; Chang, C.-H.; Lin, H.-W.; Wu, C.-C.; Fang, F.-C.; Chen, H.-F.; Wong, K.-T. *J. Mater. Chem.* **2010**, *20*, 5521. (p) Yang, C.-H.; Beltran, J.; Lemaur, V.; Cornil, J.; Hartmann, D.; Sarfert, W.; Fröhlich, R.; Bizzarri, C.; De Cola, L. *Inorg. Chem.* **2010**, *49*, 9891. (q) Chen, H.-F.; Wong, K.-T.; Liu, Y.-H.; Wang, Y.; Cheng, Y.-M.; Chung, M.-W.; Chou, P.-T.; Su, H.-C. *J. Mater. Chem.* **2011**, *21*, 768.

(3) (a) Slinker, J. D.; Gorodetsky, A. A.; Lowry, M. S.; Wang, J.; Parker, S.; Rohl, R.; Bernhard, S.; Malliaras, G. G. *J. Am. Chem. Soc.* **2004**, *126*, 2763. (b) Hu, T.; He, L.; Duan, L.; Qui, Y. *J. Mater. Chem.* **2012**, *22*, 4206.

(4) Kalyuzhny, G.; Buda, M.; McNeill, J.; Barbara, P.; Bard, A. J. *J. Am. Chem. Soc.* **2003**, *125*, 6272.

(5) (a) Bolink, H. J.; Coronado, E.; Costa, R. D.; Ortí, E.; Sessolo, M.; Graber, S.; Doyle, K.; Neuburger, M.; Housecroft, C. E.; Constable, E. C. *Adv. Mater.* **2008**, *20*, 3910. (b) Graber, S.; Doyle, K.; Neuburger, M.; Housecroft, C. E.; Constable, E. C.; Costa, R. D.; Ortí, E.; Repetto, D.; Bolink, H. J. *J. Am. Chem. Soc.* **2008**, *130*, 14944. (c) Lenes, M.; Garcia-Belmonte, G.; Tordera, D.; Pertegás, A.; Bisquert, J.; Bolink, H. J. *Adv. Funct. Mater.* **2011**, *21*, 1581. (d) Tordera, D.; Meier, S.; Lenes, M.; Costa, R. D.; Ortí, E.; Sarfert, W.; Bolink, H. J. *Adv. Mater.* **2012**, *24*, 897.

(6) (a) Sun, L.; Galan, A.; Ladouceur, S.; Slinker, J. D.; Zysman-Colman, E. *J. Mater. Chem.* **2011**, *21*, 18083. (b) He, L.; Duan, L.; Qiao, J.; Zhang, D.; Wang, L.; Qiu, Y. *Chem. Commun.* **2011**, *47*, 6467. (c) Rothe, C.; Chiang, C.-J.; Jankus, V.; Abdullah, K.; Zeng, X.; Jitchati, R.; Batsanov, A. S.; Bryce, M. R.; Monkman, A. P. *Adv. Funct. Mater.* **2009**, *19*, 2038.

(7) Wong, K.-T.; Chen, R.-T.; Fang, F.-C.; Wu, C.-C.; Lin, Y.-T. *Org. Lett.* **2005**, *7*, 1979.

(8) Su, H.-C.; Fang, F.-C.; Hwu, T.-Y.; Hsieh, H.-H.; Chen, H.-F.; Lee, G.-H.; Peng, S.-M.; Wong, K.-T.; Wu, C.-C. *Adv. Funct. Mater.* **2007**, *17*, 1019.

(9) (a) Sprouse, S.; King, K. A.; Spellane, P. J.; Watts, R. J. *J. Am. Chem. Soc.* **1984**, *106*, 6647. (b) Lohse, O.; Thevenin, P.; Waldvogel, E. *Synlett* **1999**, *1*, 45. (c) Nonoyama, M. *Bull. Chem. Soc. Jpn.* **1974**, *47*, 767.

(10) Otwinowski, Z.; Minor, W. In *Methods in Enzymology: Macromolecular Crystallography, Part A*; Carter, C. W., Jr., Sweet, R. M., Eds; Academic Press: San Diego; Vol. *276*, 2005.

(11) Sheldrick, G. M. *SHELXL-97, Program for the Solution of Crystal Structures*; University of Göttingen: Göttingen, Germany, 1997.

(12) Parker, S. T.; Slinker, J. D.; Lowry, M. S.; Cox, M. P.; Bernhard, S.; Malliaras, G. G. *Chem. Mater.* **2005**, *17*, 3187.

(13) (a) Lee, C.; Yang, W.; Parr, R. G. *Phys. Rev. B* **1988**, *37*, 785. (b) Becke, A. D. *J. Chem. Phys.* **1993**, *98*, 5648.

(14) (a) Hay, P. J.; Wadt, W. R. *J. Chem. Phys.* **1985**, *82*, 270. (b) Wadt, W. R.; Hay, P. J. *J. Chem. Phys.* **1985**, *82*, 284. (c) Hay, P. J.; Wadt, W. R. *J. Chem. Phys.* **1985**, *82*, 299.

(15) Hariharan, P. C.; Pople, J. A. *Mol. Phys.* **1974**, *27*, 209.

(16) Abrahamsson, M.; Lundqvist, M. J.; Wolpher, H.; Johansson, O.; Eriksson, L.; Bergquist, J.; Rasmussen, T.; Becker, H.-C.; Hammarstroem, L.; Norrby, P.-O.; Akermark, B.; Persson, P. *Inorg. Chem.* **2008**, *47*, 3540.

(17) Cances, M. T.; Mennucci, B.; Tomasi, J. *J. Chem. Phys.* **1997**, *107*, 3032.

(18) Lowry, M. S.; Goldsmith, J. I.; Slinker, J. D.; Rohl, R.; Pascal, R. A., Jr.; Malliaras, G. G.; Bernhard, S. *Chem. Mater.* **2005**, *17*, 5712.

(19) Costa, R. D.; Ortí, E.; Bolink, H. J.; Graber, S.; Housecroft, C. E.; Neuburger, M.; Schaffner, S.; Constable, E. C. *Chem. Commun.* **2009**, 2029.